Multi-Fidelity Multidisciplinary Whole Engine Thermo-Mechanical Design Optimization

Multi-Fidelity Multidisciplinary Whole Engine Thermo-Mechanical Design Optimization

David J.J. Toal[1] and Andy J. Keane[2]
University of Southampton, Southampton, SO17 1BJ, U.K.

Diego Benito and Jeffery A. Dixon[3]
Rolls-Royce Plc., Derby, DE24 9HY, U.K.

Jingbin Yang and Matthew Price
Rolls-Royce Plc., Bristol, BS34 7QE, U.K.

Trevor Robinson[4]
Queen's University Belfast, Belfast, BT9 5AH, U.K.

Alain Remouchamps and Norbert Kill
LMS Samtech, a Siemens business, Liege, Belgium

Traditionally the optimization of a turbomachinery engine casing for tip clearance has involved either 2D transient thermo-mechanical simulations or 3D mechanical simulations. The following paper illustrates that 3D transient whole engine thermo-mechanical simulations can be used within tip clearance optimizations and that the efficiency of such optimizations can be improved when a multi-fidelity surrogate modeling approach is employed. These simulations are employed in conjunction with a rotor sub-optimization utilizing surrogate models of rotordynamics performance, stress, mass and transient displacements and an engine parameterization.

---

[1] Senior Research Fellow, Faculty of Engineering & Environment
[2] Professor, Faculty of Engineering & Environment
[3] Chief of Thermal Systems
[4] Lecturer, School of Mechanical & Aerospace Engineering

Nomenclature

$\boldsymbol{C}$ = Co-Kriging correlation matrix

d = No. of dimensions

$\boldsymbol{d}$ = Difference between expensive and cheap data

$E[I(\boldsymbol{x}^*)]$ = Expected improvement at $\boldsymbol{x}^*$

f = Analytical test function

p = Hyperparameter controlling degree of smoothness

$\boldsymbol{R}$ = Kriging correlation matrix

s^2 = Estimate of mean square error

$\boldsymbol{x}$ = Vector of design parameters

$\boldsymbol{X}$ = Complete sampling plan

$\boldsymbol{y}$ = Vector of objective function values

θ = Hyperparameter controlling rate of correlation decrease

μ = Mean

ρ = Co-Kriging scaling factor

σ^2 = Variance

ϕ = Concentrated log-likelihood

Subscripts:

c = Cheap function

d = Difference function

e = Expensive function

I. Introduction

Modern gas turbine engine design is a continual battle to reduce emissions, fuel consumption, cost and noise. In this drive for improved performance, design optimization techniques are increasingly being seen as an important tool for finding novel designs. Any design optimization, however, is only as good as the simulation, or simulations, used to assess the performance of each design. In order to correctly model the interactions between each of the major sub-assemblies defining a gas turbine it is necessary, for example, to employ a whole engine model which models not only me-

chanical but also thermal loads. Such simulations are extremely expensive to perform and therefore difficult to encapsulate within an effective design optimization.

The following paper aims to demonstrate the feasibility of employing whole engine transient thermo-mechanical simulations within an automated design optimization loop towards the exit of the preliminary design phase. The movement of such high fidelity analyzes to this stage in the design cycle aims to improve the level of continuity between the preliminary and detailed design stages while reducing the amount of rework required during detailed design where costs are considerably higher.

The presented whole engine design optimization demonstrates a number of novel concepts which, to the authors' knowledge, have never before been employed in such an optimization. These include the application of whole engine transient thermo-mechanical simulations in the optimization of a gas turbine, a multi-fidelity surrogate modeling approach to this design optimization, a parameterization of the engine capable of maintaining the correct boundary condition tags and a multi-disciplinary sub-optimization of the rotor.

A. Specific Fuel Consumption Optimization

The overall aim of the presented design optimization is to reduce the specific fuel consumption (SFC) of the presented test engine by improving the high pressure compressor tip clearances. As demonstrated throughout the literature,[1–4] the clearance between the casing and the tip of a compressor or turbine blade has a considerable impact on the fuel consumption of an engine. While efforts have been made in the past to control the impact of these clearances through changes in casing shape or topology,[1, 5] previous studies have employed either simplified shell models of the whole engine in a mechanical analysis[5] or a combination of 2D axisymmetric transient whole engine analysis and 3D blading and rotor/stator deformations[3]. Only using a fully transient thermo-mechanical simulation of the whole engine can tip clearances be accurately predicted[2, 3]. While Benito et al.[2] presented the prediction of local tip clearances using 3D transient thermo-mechanical simulations, this analysis was not used within an optimization to drive design improvements and the analysis was restricted to only the intermediate pressure (IP) compressor casing. The design

optimization presented within this paper aims to employ simulations of a similar fidelity to those of Benito et al.[2] to improve tip clearances and therefore SFC.

As discussed by Benito et al.[2] and Arkhipov et al.[3], whole engine transient thermo-mechanical (WETTM) analyzes can be considerably expensive to perform. In order to make the application of such simulations feasible within a design optimization, either the simulation needs to be as cheap as possible (including both the runtime and the setup time) or the number of such simulations performed needs to be minimized. In general, the cost of any finite element analysis (FEA) can be controlled through a reduction in the number of degrees of freedom of the mesh. The scheme of Makem et al.[6], for example, has already been demonstrated to offer a considerable reduction in the number of degrees of freedom when meshing part of the presented test engine and could be employed along with the approaches discussed in the present paper to further reduce the cost of any SFC optimization.

B. Surrogate Modeling

The direct application of global optimization schemes, such as genetic algorithms[7] or simulated annealing[8] is completely infeasible in this case. Such schemes can require many thousands of function evaluations to successfully converge to the global optimum. Even with the analysis of many WETTM simulations in parallel on a compute cluster, the optimization would still take several months to perform.

An alternative approach is to generate a surrogate model from a relatively small number of simulations distributed throughout the design space. Surrogate models, otherwise known as response surfaces or metamodels, aim to provide an analytical representation of the response of a quantity of interest throughout the design space. Due to their analytical nature, such surrogates can be searched cheaply using a global optimization algorithm. The application of a surrogate model predicting SFC would therefore considerably reduce the number of WETTM simulations required. A similar approach was adopted by Voutchkov et al.[5] with surrogate models of SFC, mass and other objectives used to drive a multi-objective optimization.

The performance of a surrogate assisted design optimization is generally related to the accuracy

with which the surrogate predicts the true response. If the response is well predicted, the optimization can quickly find a promising design. However, if the surrogate is inaccurate, the optimization can waste evaluations of the true function improving the model and exploring the design space before converging. A simple way of improving the accuracy of any surrogate model is to include more data within that model. This, however, translates to more WETTM simulations and therefore an increase in the cost of the optimization.

An alternative is to employ a multi-fidelity approach whereby information from a small number of high fidelity simulations is augmented by additional information from a large number of lower fidelity simulations. Multi-fidelity approaches have been successfully employed throughout the literature[9–13] and have been demonstrated to be very effective at improving the quality of the final design or reducing the total simulation effort required during an optimization, compared to the low- and high-fidelity design, respectively. In the following paper we explore the application of such a multi-fidelity approach to whole engine optimization.

C. Whole Engine Parametrization

The ability to perform batch modifications of geometry is one of the main cornerstones of any engineering design optimization. Modern computer aided design (CAD) software offers the ability to create parametric models which can be easily manipulated by, for example, altering the magnitude of a dimension. While the modification of the geometry is a trivial matter, maintaining the links between this geometry and the simulation(s) used to asses the performance of the design can pose a number of significant problems. This is especially the case if the topology of the geometry changes. To maintain continuity, even in the face of such changes, a programmatic approach to the parameterization was adopted, with the presented test engine parameterization developed using the Siemens NX Open C application programming interface (API).The NX Open C API is a flexible and powerful programming interface included within the Siemens NX CAD software package[43] which gives the user access to all of the software's capabilities and has been used in the past to create flexible parametric geometry[14] and feature extraction systems[6, 15, 16].

D. Multi-Disciplinary Rotor Sub-Optimization

The tip clearance within a compressor or turbine is a function of both the movement of the casing and the rotor. In the case of Voutchkov et al.[5], the design of the rotor was fixed and only the casing design was changed as part of the optimization. In the present optimization, a bi-level approach is taken whereby for every new casing considered the rotor is redesigned in a sub-optimization. This sub-optimization takes into account constraints on rotor mass, stress and rotordynamics performance when maximizing overall engine SFC. Such an approach results in an active trade-off between rotor and casing mass. As the top level optimization progresses, mass removed from the rotor can be used to improve the stiffness of the casing and vice versa.

Of course, any analysis performed as part of the rotor sub-optimization will increase the total time spent evaluating each new casing design. Given that an identical rotor sub-optimization is performed for every new casing design, surrogate models of rotor stress, mass and rotordynamics performance can be easily substituted thereby considerably reducing the sub-optimization cost. The change in tip clearance and therefore the change in SFC with each new rotor design is dependent on the displacement of the casing. As this is not known before the WETTM analysis is performed, it is impossible to construct a surrogate model of rotor SFC a priori. Instead the presented optimization employs a novel surrogate modeling approach to predict the transient displacements of the compressor blade platforms modeled in the rotor simulation. The rotor sub-optimization therefore uses this surrogate model to predict the platform displacements for each rotor design which can then be combined with the displacements of the casing from the WETTM simulation to calculate tip clearance and therefore SFC.

E. Optimization Strategy Overview

To summarize, the optimization presented within this paper and illustrated graphically in Figure 1, employs an NX Open C based parameterization of the test engine which maintains continuity between the engine geometry and the boundary conditions of the FEA simulation. With a new engine generated from the parametric model the design is passed to a whole engine transient thermo-mechanical simulation, or if a multi-fidelity approach is adopted, a whole engine steady-state

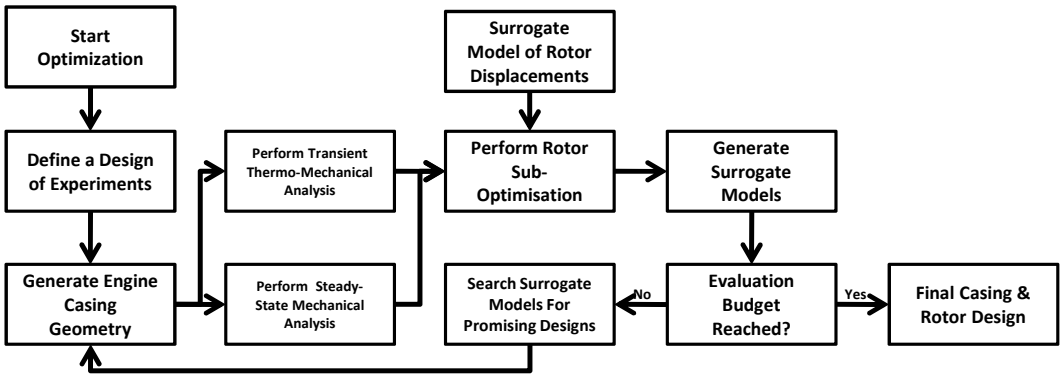

Fig. 1 Multi-fidelity optimization workflow.

mechanical simulation. Displacements from these simulations are used in conjunction with surrogate models predicting transient displacements, mass, stress and rotordynamics performance in a rotor sub-optimization. The resulting SFCs and total engine masses are then used to construct surrogate models which are used in a global optimization. Promising casing designs are then assessed and used to improve the accuracy of the surrogates with the process repeating until a predefined stopping criterion has been reached.

Given the importance of single and multi-fidelity surrogate modelling to the optimizations considered, the following article begins by describing in detail the mathematics behind both Kriging and, its multi-fidelity variant, Co-Kriging. The parametric model of the test engine is then described before the various simulations and post-processing operations are considered in turn. The transient thermo-mechanical simulations of the static engine casings and rotors are discussed and the post-processing operations used to calculate the SFC of each new engine design are described. Finally, the details of the 2D rotordynamics simulation are presented before being applied in conjunction with the thermo-mechanical simulations in a simple two variable optimization of the rotor. The methodologies used in the construction of the surrogates used in the rotor sub-optimizations are presented and their accuracy assessed. A comparison of the global accuracy of single and multi-fidelity surrogate models of engine SFC is then presented before these methods are compared using four and ten variable bi-level optimizations of the whole engine.

II. Kriging & Co-Kriging

Popularized by Sacks et al.[17] for use in the prediction of deterministic computational responses, Kriging, of the surrogate modeling techniques within the literature[18–20], is perhaps one of the most popular due to its predictive accuracy and useful prediction of the error in the model.

A Kriging model is constructed based on the assumption that when two points are close together in the design space their objective function values will be similar. This is modeled by assuming that the correlation between two points $\boldsymbol{x}_i$ and $\boldsymbol{x}_j$ is

$$\boldsymbol{R}_{ij} = \mathrm{Corr}\left[Y(\boldsymbol{x}_i), Y(\boldsymbol{x}_j)\right] = \exp\left(-\sum_{l=1}^{d} 10^{\boldsymbol{\theta}^{(l)}} \|\boldsymbol{x}_i^{(l)} - \boldsymbol{x}_j^{(l)}\|^{\boldsymbol{p}^{(l)}}\right), \tag{1}$$

where $\boldsymbol{\theta}^{(l)}$ and $\boldsymbol{p}^{(l)}$ represent the, so called, hyperparameters of the l^{th} design variable and define the rate of correlation decrease and the degree of smoothness, respectively. These hyperparameters are defined through a maximization of the likelihood on the observed dataset, $\boldsymbol{y}$, which, after simplification[21], equates to

$$\phi = -\frac{n}{2}\ln(\hat{\sigma}^2) - \frac{1}{2}\ln(|\boldsymbol{R}|), \tag{2}$$

with

$$\hat{\sigma}^2 = \frac{1}{n}(\boldsymbol{y} - \mathbf{1}\hat{\mu})^T \boldsymbol{R}^{-1}(\boldsymbol{y} - \mathbf{1}\hat{\mu}) \tag{3}$$

and

$$\hat{\mu} = \frac{\mathbf{1}^T \boldsymbol{R}^{-1} \boldsymbol{y}}{\mathbf{1}^T \boldsymbol{R}^{-1} \mathbf{1}} \tag{4}$$

defining maximum likelihood estimates of the variance, $\hat{\sigma}^2$ and mean, $\hat{\mu}$, respectively. A hybridized particle swarm algorithm, similar to that of Toal et al.[22], is employed within the surrogate modeling toolbox of the proprietary optimization software, OPTIMATv2[5, 22–25], to optimize the hyperparameters in all Kriging and Co-Kriging models presented within this article.

Given an optimal set of hyperparameters, the vector of correlations, $\boldsymbol{r}(\boldsymbol{x}^*)$, between an unknown point, $\boldsymbol{x}^*$, and the known sample points can be used in conjunction with the mean to calculate the prediction of the Kriging model at the unknown point,

$$y(\boldsymbol{x}^*) = \hat{\mu} + \boldsymbol{r}^T \boldsymbol{R}^{-1}(\boldsymbol{y} - \mathbf{1}\hat{\mu}). \tag{5}$$

This predictor can be used by any global optimization routine to search the design space for an optimum. Alternatively an estimate of the mean square error of the Kriging model,

$$s^2(\boldsymbol{x}^*) = \hat{\sigma}^2 \left[1 - \boldsymbol{r}^T \boldsymbol{R}^{-1} \boldsymbol{r}\right], \tag{6}$$

can also be calculated at an unknown point and used to update the surrogate model in areas of maximum error thereby improving the model's global accuracy. This error estimate can also be employed in another popular updating criterion - expected improvement ([26]),

$$E[I(\boldsymbol{x}^*)] = \frac{(y_{\min} - y(\boldsymbol{x}^*))}{2}\left[1 + \operatorname{erf}\left(\frac{y_{\min} - y(\boldsymbol{x}^*)}{s\sqrt{2}}\right)\right] + \frac{s}{\sqrt{2\pi}} \exp\left[\frac{-(y_{\min} - y(\boldsymbol{x}^*))^2}{2s^2}\right]. \tag{7}$$

Here erf() denotes the error function and $y_{\min}$ denotes the objective function value of the best unconstrained design found so far. An exhaustive search of the expected improvement over a design space attempts to locate an update point which is most likely to result in an improvement over the current best design and therefore attempts to balance both exploration and exploitation of the design space. Evaluating the true objective function at the optimum indicated by the predictor can result in the optimization becoming trapped in a local minimum thereby resulting in a sub-optimal design. Using the expected improvement update criterion, on the other hand, has been demonstrated[21, 26] to allow the optimization to escape from such local optima thereby guaranteeing that the global optimum will be reached if given enough function evaluations.

Co-Kriging extends the Kriging concept described above to deal with multiple levels of simulation fidelity. Using the approach of Kennedy and O'Hagan,[27] the high fidelity response is approximated by multiplying a Gaussian process representing the low fidelity response by a scaling factor, ρ, and adding a second Gaussian process of the difference between the high and low fidelity data,

$$Z_e(\boldsymbol{x}) = \rho Z_c(\boldsymbol{x}) + Z_d(\boldsymbol{x}). \tag{8}$$

If $\boldsymbol{X}_e$ and $\boldsymbol{X}_c$ represent the expensive and cheap data respectively, then the covariance matrix $\boldsymbol{C}$ is

$$\boldsymbol{C} = \begin{pmatrix} \sigma_c^2 \boldsymbol{R}_c(\boldsymbol{X}_c, \boldsymbol{X}_c) & \rho\sigma_c^2 \boldsymbol{R}_c(\boldsymbol{X}_c, \boldsymbol{X}_e) \\ \rho\sigma_c^2 \boldsymbol{R}_c(\boldsymbol{X}_e, \boldsymbol{X}_c) & \rho^2\sigma_c^2 \boldsymbol{R}_c(\boldsymbol{X}_e, \boldsymbol{X}_e) + \sigma_d^2 \boldsymbol{R}_d(\boldsymbol{X}_e, \boldsymbol{X}_e), \end{pmatrix} \tag{9}$$

where the correlations are assumed to be of the same form as Eq. 1. Given that there are now two Gaussian processes in the model, there are twice as many hyperparameters to determine compared to the standard Kriging model above. The scaling parameter ρ must also be determined.

As the low fidelity data is considered to be independent of the high fidelity data, the same maximization of likelihood process used to determine the hyperparameters for the standard Kriging model can be employed. The hyperparmeters of the difference model can then be optimized using a similar process but with the objective function $\boldsymbol{y}$ replaced by the difference between the expensive and scaled cheap data,

$$\boldsymbol{d} = \boldsymbol{y}_e - \rho \boldsymbol{y}_c(\boldsymbol{X}_e). \tag{10}$$

With the hyperparameters optimized, the covariance matrix, Eq. 9, can be calculated and used in conjunction with a column vector, $\boldsymbol{c}$, of covariances of an unknown point to the known points to predict the high fidelity response at that unknown point,

$$y_e(\boldsymbol{x}^*) = \hat{\mu} + \boldsymbol{c}^T \boldsymbol{C}^{-1}(\boldsymbol{y} - \boldsymbol{1}\hat{\mu}), \tag{11}$$

with the mean now,

$$\hat{\mu} = \frac{\boldsymbol{1}^T \boldsymbol{C}^{-1} \boldsymbol{Y}}{\boldsymbol{1}^T \boldsymbol{C}^{-1} \boldsymbol{1}}, \tag{12}$$

where $\boldsymbol{Y}$ is a combination of the known low and high fidelity responses. As per the standard Kriging model, the Co-Kriging model provides an estimate of the mean square error,

$$s_e^2(\boldsymbol{x}^*) = \rho^2 \hat{\sigma}_c^2 + \hat{\sigma}_d^2 - \boldsymbol{c}^T \boldsymbol{C}^{-1} \boldsymbol{c} + \frac{1 - \boldsymbol{1}^T \boldsymbol{C}^{-1} \boldsymbol{c}}{\boldsymbol{1}^T \boldsymbol{C}^{-1} \boldsymbol{1}}, \tag{13}$$

which can be used in the calculation of expected improvement[28].

Figure 2 helps to illustrate the advantages of Co-Kriging over Kriging in the prediction of a simple one dimensional analytical test function. The thick solid black line of Figure 2 represents a high fidelity, or expensive, function,

$$f_e = (6x - 2)^2 \sin(12x - 4), \tag{14}$$

while the thinner solid black line represents a low fidelity, or cheap, function,

$$f_c = 0.5 f_e + 10(x - 0.5) - 5. \tag{15}$$

Constructing a Kriging model using the four expensive design of experiments (DoE) points illustrated results in a surrogate model which does not accurately represent the true function and would

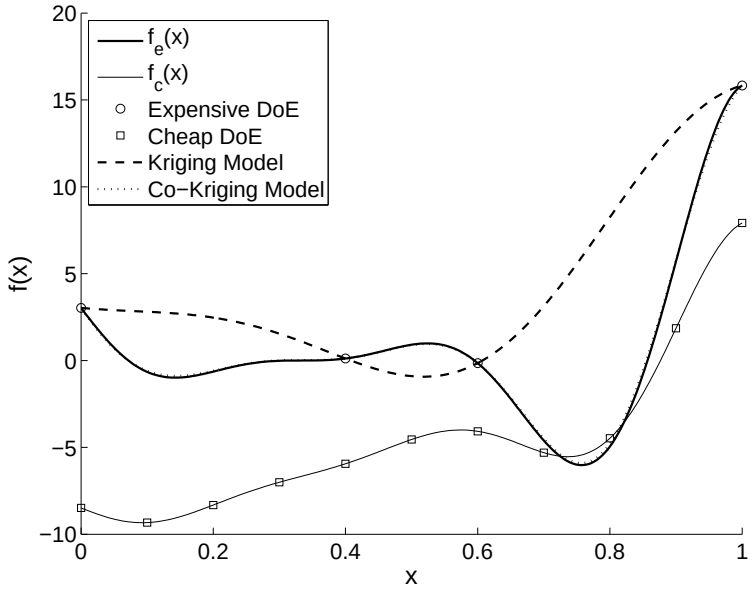

Fig. 2 Analytical example of Kriging Co-Kriging (recreated from Forrester et al.[28]).

mislead any optimization. However, combining 11 additional data points evaluated using the low fidelity function with the same four expensive points produces a surrogate model which very accurately represents the true function. In fact, the Co-Kriging prediction is almost indiscernible from the true function. In this case the likelihood optimization for the difference model results in a value of $\rho \approx 2$ thereby producing a difference model which reduces linearly in magnitude from $x = 0$ to $x = 1$. When this model is combined with the cheap prediction this has the effect of increasing the magnitude of the cheap function more, closer to $x = 0$ than to $x = 1$ which therefore translates the cheap function into something closely resembling the expensive function.

III. Test Engine & Parameterization

The majority of engineering design optimizations assess the performance of a new design using some form of computational simulation. Be it computational fluid dynamics or finite element analysis, generally these simulations require some form of discretized geometry as an input. Modifications to the geometry are then reflected in the mesh and therefore in the results of the simulation which

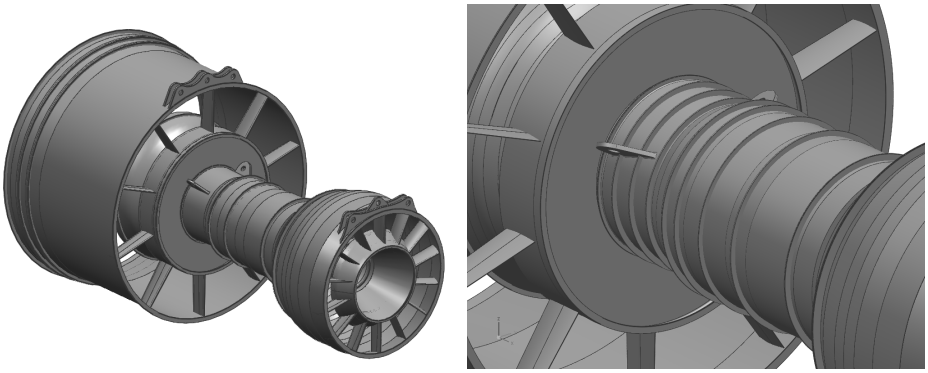

(a) (b)

Fig. 3 Baseline 3D engine casing (a) and compressor intercasing with additional stiffening rings and modified thrust linkages (b).

indicates if the modification was successful. The task of creating the simulation model from the geometry can be in itself an expensive process, and the objective must be to automatically propagate the analysis information from one analysis model to the next iteration. Whilst the ability to modify geometry is important in its own right, ensuring that the modified geometry is still compatible with the simulation is perhaps more important and, in some cases, can be difficult to achieve. If the model is not compatible with the previous simulation setup, the amount of manual effort required to make it so can make the entire process infeasible.

Consider for example the baseline engine design illustrated in Figure 3(a). In order to perform a WETTM simulation of this engine geometry, boundary conditions must be applied to every face of the illustrated solid body. To achieve this, each face is "tagged" or "named" within the CAD environment with these tags then being used to assign boundary conditions within the FEA simulation. Naturally, if any of these tags should be altered or deleted, the boundary conditions would not be applied correctly and either the simulation would fail or, perhaps more seriously, the simulation would complete successfully but the results would be unreliable. Within an automated design optimization loop, where there can be minimal human intervention, such issues can result in the optimization being led into the incorrect region of the design space. Given the cost of the

WETTM simulations employed here, this is something that must be avoided at all costs.

Such issues can be avoided by using the CAD package in one of two ways. The optimization can be constrained to only consider modifications to the geometry which do not result in changes that alter the geometry tags. However, this is almost impossible to identify a priori and, where enforced, it would restrict modifications of engine to changes in casing thickness, flange heights and widths and some topological changes such as the number of aerodynamic struts at the compressor exit. Unfortunately the inclusion of additional stiffening rings around the casing, which may possibly offer improvements in tip clearance and SFC could not be investigated. The inclusion of such a feature results in a split along the cylindrical face to which it is attached thereby creating a new cylindrical face with no tag and therefore no associated boundary conditions. Nolan et al.[16] describe a method for defining boundary conditions on computed interfaces so that they can be propagated onto new topological faces when they occur, but this requires the model to be represented in a certain way.

The second approach is to create the parametric model in such a manner as to embed intelligence regarding the boundary condition tags so that if topology changes are sufficient to remove tags or result in faces with no tags this can be accounted for and automatically corrected. Given that the eventual design optimization aims to explore topology changes such as the inclusion of additional stiffening rings this is the approach that is taken here.

The parameterization of the test engine illustrated in 3(a) was developed using the Siemens NX6 Open C API. Rather than create the geometry in a traditional manner using the graphical user interface (GUI), the operations to create or modify the geometry were written into a C program which could be run from within NX. As the high pressure compressor (HPC) casing, illustrated in Figure 3(b), was the main subject of the WETTM optimization, it was important to make the parameterization as flexible as possible. The Open C program therefore contained all of the commands to create the HPC casing from scratch. This included operations, for example, to draw lines and revolve them to create casing faces, create blends between flanges and casings and extrude aerodynamic stiffeners. By altering the values contained within a simple text file more than 30 parameters defining the shape of the HPC casing could be altered including casing thicknesses, flange heights and widths (see Figure 4), the position, number and size of internal aerodynamic

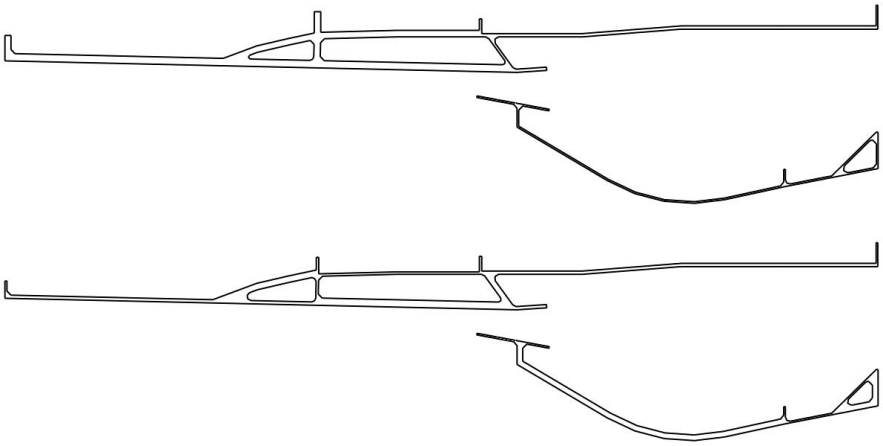

Fig. 4 Example modifications to casing thicknesses and stiffener thicknesses and heights.

struts and the circumferential position and setting angle of thrust linkages (see Figure 3(b)). The process of generating the geometry completely from scratch using the Open C program each time is, in this case, insignificant compared to the cost of the FE analysis.

As well as these changes, the input file will also control the addition of n fully parametric stiffening rings applied to the outer faces of the HPC casing. The position, height and thickness of each additional stiffening ring can be controlled via the input file. Figure 3(b) illustrates the modification of the baseline HPC casing geometry shown in Figure 3(a) through the addition of six additional stiffening rings to the casing.

As described above, the addition of stiffening rings in such a manner will typically result in the creation of new cylindrical faces with no tags. When the rings are applied in this instance, the creation and modification of faces is tracked and the new face has the correct tag applied. By employing an NX Open C geometry parameterization, the tags, and therefore the correct application of boundary conditions, can be explicitly accounted for and issues arising from such topology changes can be minimized.

The test engine geometry consists of a total of five separate solid bodies: the fan casing, HPC

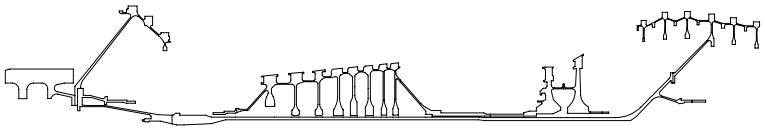

Fig. 5 Two dimensional rotor geometry.

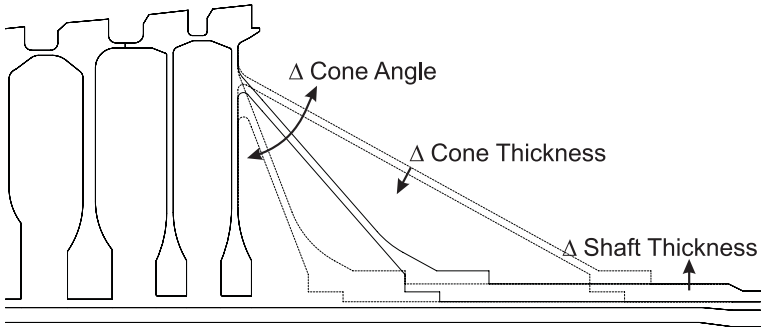

Fig. 6 Illustration of the rear HPC rotor parameterization.

casing, high pressure turbine (HPT) casing, low pressure turbine (LPT) casing and turbine bearing struts. Of these solid bodies, only the HPC casing is completely parametric with the baseline HPT, LPT and struts read into the model unaltered. While the main part of the fan casing is read in unaltered, the Open C program is used to apply a fully parametric fan case mounting bracket to the top of the casing. While the ability to modify the location of the mount is embedded within the Open C program it, is not employed in any of the optimizations presented within this paper.

As previously stated, the WETTM optimization aims to employ a sub-optimization of the rotor. In order to perform this optimization, or in this case, generate the information necessary to create the surrogate models to perform the optimization, a geometry parameterization is required.

As per the casing parameterization described above, the 2D rotor, illustrated in Figure 5 is parameterized using an NX Open C program. In this case, the angle and thickness of the rear HPC cone and the thickness of the shaft can vary. With a simple text file, once again, used to alter the design parameters. Figure 6 illustrates the extent of the modifications to the rotor which can be

made.

IV. Transient Thermo-Mechanical Simulations

As briefly noted in the introduction, the performance of the test engine is assessed using a transient thermo-mechanical analysis. The setup of this analysis closely follows the work of Benito et al.[2] with all engine casings simulated simultaneously rather than just the IP compressor casing.

The WETTM analysis is performed using the proprietary Rolls-Royce FEA package SC03, a description of which can be found in Armstrong and Edmunds[29]. SC03, in this case, is used to perform the analysis and pre-process the engine geometry generated by the NX Open C program. Upon creation of the geometry in NX, a Parasolid file is exported before CADfix is used to convert the Parasolid into SC03's native geometry input format. SC03 then reads in the geometry and generates a 3D fully unstructured mesh consisting of ten node, second order, tetrahedral elements. An SC03 mesh of the baseline engine consists of approximately 900k elements and 1.79m nodes.

The engine is simulated over a so called "square cycle" comprising conditions at idle followed by an acceleration to max take-off (MTO) and then a deceleration to idle and then an acceleration to cruise. Stabilization periods of 2000 seconds are employed at MTO and at cruise. In addition to these conditions a gust event is simulated at cruise and a rotation event is simulated at MTO.

As per the work of Benito et al.[2], thermal boundary conditions have been applied to each of the model's faces to represent convective heat transfer and radiation. With pressures, temperatures, heat transfer coefficients and flow directions specified for both oil and air at all of the conditions outlined above. Including meshing of the geometry, the 3D WETTM simulation takes approximately 104 hours to perform on an eight core node of the University of Southampton's Spitfire cluster using SC03 version 13.

As outlined in the introduction, one of the focuses of this paper is to assess the application of a multi-fidelity approach to accelerate the optimization. A lower fidelity version of the 3D WETTM simulation is therefore required to perform such an optimization. In this case, through a simple setting change in SC03, the WETTM simulation is converted into a steady state mechanical simulation. This simulation uses an identical mesh to that employed during the WETTM simulations

but only mechanical loads are considered at the predefined points of the cycle. This reduces the cost of the simulation from 104 hours to approximately 3.4 hours, which equates to less than $1/30^{\text{th}}$ the cost of the full fidelity WETTM simulation.

As described previously, the calculation of tip clearances requires displacement information for both the casing and the rotor. Due to its axisymmetric nature, the rotor is simulated in two dimensions only. The rotor is simulated over the exact same cycle as the 3D casing simulation and employs a total of 3494, second order, six node triangular elements. Given its 2D nature and relatively small numbers of degrees of freedom, a single transient analysis of the rotor can be performed on a desktop computer in well under 5 minutes.

V. Calculation of SFC

The successful completion of a 3D WETTM simulation and a 2D rotor simulation results in temperatures and displacements across all of the static and rotating parts of the engine for a square cycle, which can be over 120 time steps. This information must be condensed into a single number by which the effectiveness of the casing and rotor design can be judged. To do this the transient casing and rotor displacements are first converted into a measure of the effective running clearance at cruise. This information is then used to determine a change in the efficiency of the compressor which is used in a PROOSIS (PRopulsion Object-Oriented SImulation Software)[30, 31] model of the test engine.

The calculation of the effective running clearance begins in a manner similar to that used by Benito et al.[2] to perform a "roundness assessment" of the IP compressor casing. Upon completion of the 3D WETTM simulation, displacements at 64 reference points equally spaced around the circumference of the front and rear rotor bearings and each of the eight compressor stages are extracted for all of the simulation time steps. Least squares circles are fitted to the displacement data for the two bearings which are used to define the location of the center of the rotor. Using these center points, the displacements of the rotor for each compressor stage is adjusted.

Given a set of rotor displacements corrected for the location of the rotor inside the casing, the closures for each compressor stage at each time step can be calculated. Using these closures, the

pinch point closure and the circumferentially averaged closure at the end of cruise is calculated for each compressor stage. The cruise running clearance is then defined as the difference between the pinch point closure and the average cruise closure. This clearance is then non-dimensionalized by the height of the blade for each stage and the root mean square taken across the eight stages to calculate the effective running clearance of the compressor at cruise.

With the effective running clearance calculated for any new design considered, it is compared to the baseline design with a 1% change in running clearance assumed to directly translate to a 1% change in compressor efficiency. This, of course, is a rather simple assumption and fails to take into account all of the factors which impact compressor efficiency but will be used here to translate running clearance into the more familiar metric of SFC. With the new compressor efficiency calculate the PROOSIS model of the engine can be run using this efficiency with the resulting SFC then used as the objective function within the optimization.

VI. Rotordynamics Simulation

As described in the introduction, not only will the stress, mass and effect of the rotor on SFC be considered as part of the sub-optimization but the rotordynamics performance of the rotor will also be analyzed, in this case using SAMCEF Rotors, a software tool dedicated to the analysis of rotating machines[44].

The rotordynamics model, in this case, is based on 2D Fourier multi-harmonic elements whose material properties are temperature dependent. The 2D transient thermo-mechanical simulation of the rotor described previously is run first and used to provide the 2D temperature mapping to define the material properties. Only rotor temperatures during cruise were mapped to the rotordynamics model but the same process could be repeated at other points in the operating cycle. With the temperatures mapped, a critical speed analysis was performed to generate the Campbell diagram.

Upon completion of a successful rotordynamics simulation, the output file, which contains the Campbell diagram, is parsed to calculate all critical speeds. These critical speeds are then analyzed with all of the frequencies that fall outside the range of the frequency sweep used in the simulation, belonging to constant frequencies and backward whirl modes ignored. Finally the remaining

critical speeds are compared to the operating speed of the rotor at idle, cruise and MTO, with the absolute difference between the operating speed and the closest critical speed returned. Within the rotordynamics literature, this, or a similar metric, is often maximized in order to improve the rotordynamics response of the system[32–37].

VII. Two Variable Rotor Optimization & Prediction of Transient Displacements

As described in the overview of the WETTM optimization strategy, with every new casing design considered, the rotor is tailored specifically for that casing through a rotor sub-optimization. As this sub-optimization is identical in every instance that it is carried out, the sub-optimization can be accelerated considerably through the use of a series of surrogate models to represent the variation of mass, stress, critical speed and transient displacements throughout the design space.

An initial surrogate based optimization of the 2D rotor using the baseline casing design could, of course, be used to generate the necessary surrogate models for all subsequent rotor sub-optimizations. Consider therefore, the optimization of the rotor to minimize SFC while constraining the maximum rotor mass, the minimum separation between the operating speed of the rotor and the nearest critical speed to be that of the baseline design and the maximum Von Mises stress in the cone and rear two rotor discs to increase by no more than 10%. In this case, the calculation of the SFC employs a new set of displacements from each 2D rotor simulation and a fixed set of displacements from the WETTM simulation of the baseline engine casing design.

Figure 7 illustrates the search history of a two variable Kriging based optimization of the rotor. In this case, an initial 20 point sampling plan of the design space has been augmented by 15 update iterations. Each iteration of this optimization involves the construction of surrogate models for the objective function and each of the constraints followed by a genetic algorithm based optimization to maximize the expected improvement criterion[26], subject to the constraints. The design point which maximizes expected improvement is then evaluated using the simulations and the resulting objective and constraints are used to improve each of the surrogate models. With a new, updated, set of surrogates the process is repeated to find another design. The optimization results in a total of 35 transient thermo-mechanical and rotordynamics simulations for rotors with varying cone angle

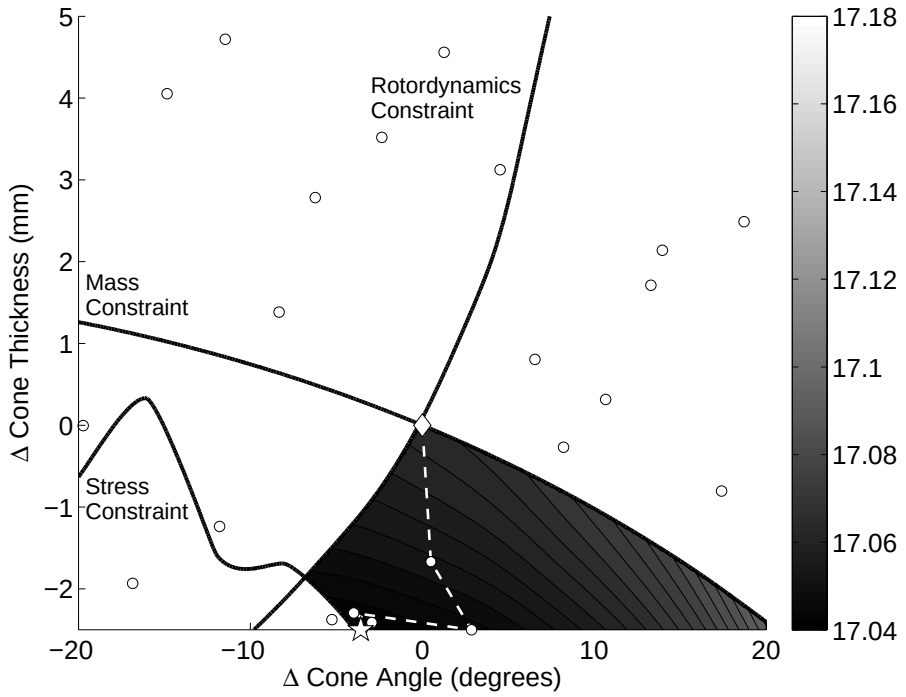

Fig. 7 Two variable rotor optimization search path.

and cone thickness and takes approximately one day on a standard desktop computer.

The contours of Figure 7 are representative of the "true" design space and have been created from surrogate models of the objective and constraints using a full factorial sampling plan with a total of 121 points. These contours illustrate the variation in SFC within the feasible region of the design space bounded by the stress, mass and rotordynamics constraints. The bounds of these constraints are represented in Figure 7 by solid black lines with the region in the bottom left corner exceeding the stress constraint, the region above the horizontal line exceeding the mass constraint and the region to the left of the vertical line exceeding the rotordynamics constraint. Figure 7 therefore illustrates that even with a modest number of simulations a surrogate based optimization can improve the baseline design (indicated by the white diamond) and efficiently find the optimum (indicated by the white star).

While the rotor optimization has resulted in a modest improvement in the SFC of the engine (approximately 0.133%), it has produced, in this case, a considerable reduction in the mass of the

Table 1 Comparison of rotor surrogate model accuracies.

	After initial optimization			After space filling updates		
	r^2	RMSE	MAE	r^2	RMSE	MAE
Rotor Mass Constraint	1.00	0.08 (0.46%)	0.53 (3.15%)	1.00	3.21×10^{-3} (0.02%)	8.46×10^{-3} (0.06%)
Rotor Stress Constraint	0.94	0.02 (5.89%)	0.086 (25.88%)	1.00	4.17×10^{-3} (1.25%)	0.01 (3.71%)
Rotordynamics Constraint	0.98	12.13 (5.04%)	45.00 (18.71%)	1.00	3.02 (1.48%)	13.46 (6.59%)
SFC Prediction	0.42	0.03 (21.00%)	0.10 (77.30%)	0.990	2.37×10^{-3} (1.77%)	7.20×10^{-3} (5.39%)

rotor (4.34kg), which could be traded off to improve the stiffness of the casing design as part of the complete optimization.

In order to effectively employ the surrogate models constructed during the above optimization of the rotor, the models should accurately represent the design space. Table 1 presents the accuracies of the surrogate models produced at the end of the rotor sub-optimization when compared to the full factorial, 121 point, sampling plan. Pearson's r^2 correlation, the root mean square error (RMSE) and maximum absolute error (MAE) for each of the surrogate models are presented in Table 1. A conversion of the RMSE and MAE into percentages of the maximum range of values in the true response are also presented so that the relative accuracy of each model can be assessed.

The results of Table 1 indicate that the general trends of the rotor mass, stress and rotordynamics constraints are well represented by their respective surrogate models at the end of the optimization. However, although each of these constraints has a high r^2 correlation, their accuracy in terms of predicting accurate magnitudes varies considerably. The mass constraint is almost linear and so is captured very well by the surrogate model with a RMSE value equating to less than 0.5% of the total variation in the true response. The MAE of 3.15% of the response is due to the absence of updates or design of experiments (DoE) points in the upper corners and the bottom left corner of the design space where the constraints are violated.

Both the stress and rotordynamics constraints appear to be more poorly represented by their respective surrogate models at the end of the optimization. Both have RMSEs of over 5% and large MAEs of over 25% and 18% for the stress and rotordynamics constraints, respectively. These errors

are due to a combination of more complex responses throughout the design space and a lack of additional update points in regions deemed to exceed the constraints.

The stress constraint, for example, exhibits a large increase in the magnitude of the stress beyond the constraint boundary illustrated in Figure 7. Without updates in this region it is very difficult for a Kriging model to predict an increase in the magnitude of the stress, instead as the model moves away from the nearest DoE point it will return to the mean value which results in the large MAE error observed in Table 1.

The rotordynamics constraint is predicted slightly better than the stress constraint but nevertheless suffers from similar issues. The large MAE occurs in a region of the design space not explored during the optimization due to it violating the constraints.

In the above optimization, the SFC of the engine is calculated based on a fixed set of displacements from a WETTM simulation of the baseline casing design and a set of displacements calculated for each rotor design. In order to avoid running TTM analyzes of the rotor as part of any eventual rotor sub-optimization, surrogate models are required which predict the transient response of the rotor as the rotor design variables change. These predicted transient responses can then be used with fixed casing displacements to calculate tip clearances and therefore SFC throughout the design space of the rotor.

The construction of such a surrogate begins by storing the transient displacements for each compressor stage as each rotor is analyzed. The transient displacements for each stage are then used to perform a proper orthogonal decomposition (POD) which results in a series of POD basis functions and corresponding modal coefficients. The variation in the magnitude of these modal coefficients throughout the rotor design space can then be predicted using a standard surrogate modeling technique such as Kriging. A similar process has been employed by [38] in the prediction of transient turbine blade and compressor casing temperatures and by [39] in the prediction of a velocity field inside the combustion chamber of a reciprocating engine. In this case, the "method of snapshots" proposed by [40] is employed with the number of modal coefficients selected so as to represent more than 99.99% of the variation.

Given that the main sources of errors of the constraint surrogates are in regions of the design

space which violate the constraints and are therefore not of interest, the surrogates resulting from the optimization could be directly used in the sub-optimization. However, as shown in Table 1, the prediction of the SFC resulting from a prediction of the transient displacements of each of the rotors is rather poor. At the end of the optimization, there is an unacceptable error in both the representation of the general trend of the SFC response and the prediction of the absolute value even in regions of interest. Upon completion of the SFC optimization, a further improvement of the prediction of the transient responses is therefore required before it can be considered to be fit for use within any sub-optimization.

To improve the accuracy of the SFC prediction, further updates were evaluated in regions of the design space not previously explored until the prediction of the SFC through the POD based transient displacement prediction became acceptable. In this case, a total of 40 additional space filling updates were required, the impact of which can be observed in Table 1 on the prediction of SFC and the three constraints. These update points were defined by searching the design space for a point which has the maximum minimum distance to a previously considered sample point. Such a "Max-Min" criteria is quite popular within the literature to define optimal space filling sampling plans[41].

The additional transient displacement information improves the POD based prediction of the transient responses and therefore considerably improves the prediction of SFC. The r^2 correlation has increased from 0.424 to 0.993 indicating that the trend in the SFC is well represented. Similarly the RMSE improves from 21% to a much more accurate 1.77% and the MAE drops from 77.3% to 5.39%. The accuracy of the SFC prediction can be observed graphically in Figure 8, where the predicted SFC can been seen to faithfully represent the "true" SFC resulting from the full factorial design.

Table 2 helps to illustrate the accuracy with which the POD based approach predicts the transient displacements for each of the eight stages of the HPC. In this case, the r^2 correlation, RMSE and MAE are calculated with respect to transient displacements from actual FEA simulations of the 121 rotors making up the full factorial design. Indicated percentage values are taken with respect to the maximum range of displacements for each stage across all 121 test rotors. Also

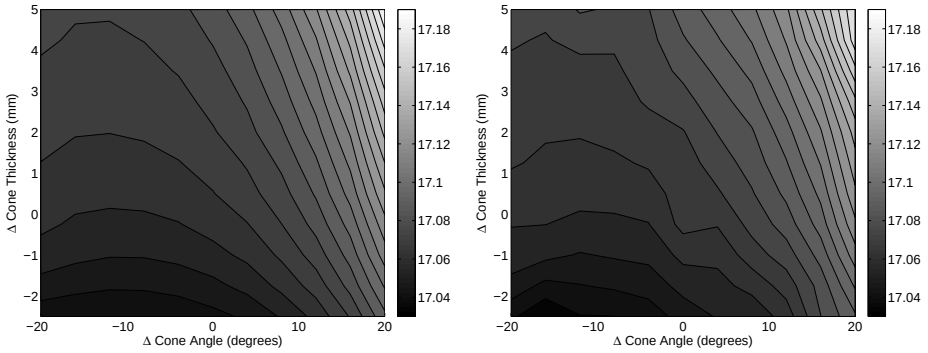

(a) (b)

Fig. 8 A graphical comparison between the true SFC throughout the rotor design space (a) and the SFC predicted using the predicted transient displacements (b).

Table 2 Number of POD modes and the accuracy of surrogate model predictions of transient rotor displacements.

	No. Modes	r^2	RMSE	MAE
Stage 1	1	1.000	1.90×10^{-5} (1.89×10^{-3}%)	4.73×10^{-4} (0.047%)
Stage 2	1	1.000	2.32×10^{-5} (1.93×10^{-3}%)	7.28×10^{-4} (0.061%)
Stage 3	1	1.000	3.26×10^{-5} (2.49×10^{-3}%)	8.83×10^{-4} (0.068%)
Stage 4	1	1.000	2.99×10^{-5} (2.09×10^{-3}%)	6.05×10^{-4} (0.042%)
Stage 5	0	1.000	1.02×10^{-4} (7.18×10^{-3}%)	5.46×10^{-4} (0.038%)
Stage 6	1	1.000	1.01×10^{-4} (6.58×10^{-3}%)	7.47×10^{-4} (0.048%)
Stage 7	5	1.000	1.20×10^{-4} (5.27×10^{-3}%)	1.18×10^{-3} (0.052%)
Stage 8	5	1.000	3.15×10^{-4} (1.27×10^{-2}%)	2.51×10^{-3} (0.101%)

indicated in Table 2 is the number of POD modes required to represent 99.99% of the variation for each compressor stage.

Generally, the transient rotor displacements are well predicted for each of the eight compressor stages with the largest observed error being 2.51×10^{-3}mm or 0.1% of the range of displacements. The calculation of effective running clearance at cruise and therefore the SFC of the engine is very

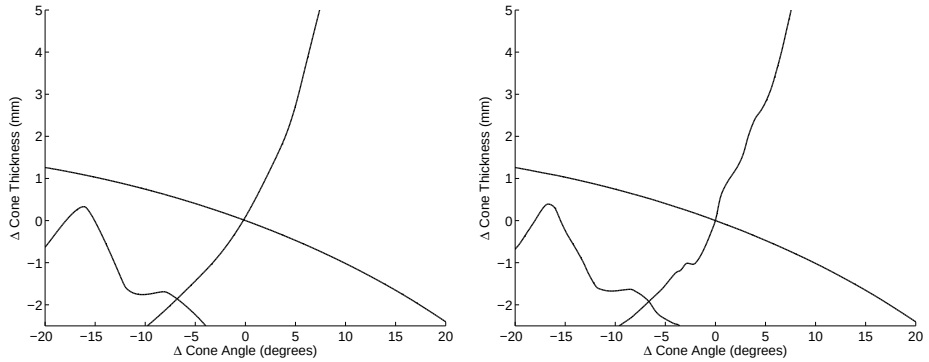

(a) (b)

Fig. 9 A graphical comparison between the true constraint boundaries (a) and the predicted constraint boundaries (b).

sensitive to slight variations in the displacements of either the casing or the rotor resulting in the relatively larger errors in the SFC prediction observed in Table 1.

Table 2 also indicates that changes to the rear cone angle and thickness, in this case, mainly affect the rear two stages of the HPC. These two stages require a larger number of POD bases to accurately capture the variation in the transient displacements between designs. The remaining stages require only one POD basis or, in the case of stage 5, just the mean.

The surrogate models representing each of the constraints are also improved through the 40 additional updates. The RMSE in the prediction of the stress and rotordynamics constraints drop from 5.89% to 1.25% and from 5.04% to 1.48%, respectively, while the MAEs drop from 25.9% to 3.7% and from 18.7% to 6.59%. Once again, the regions of maximum error are in areas where the constraints are violated and therefore not an issue.

Although the trend and magnitude of these constraints appear to be accurately predicted, how does this impact the prediction of the constraint boundaries? Figure 9 presents a comparison between the "true" constraint boundaries also presented in Figure 7 and those predicted by the surrogate models. Generally, the constraints are predicted very well, in particular, there is no discernible difference between the "true" mass constraint boundary and that predicted by its surrogate

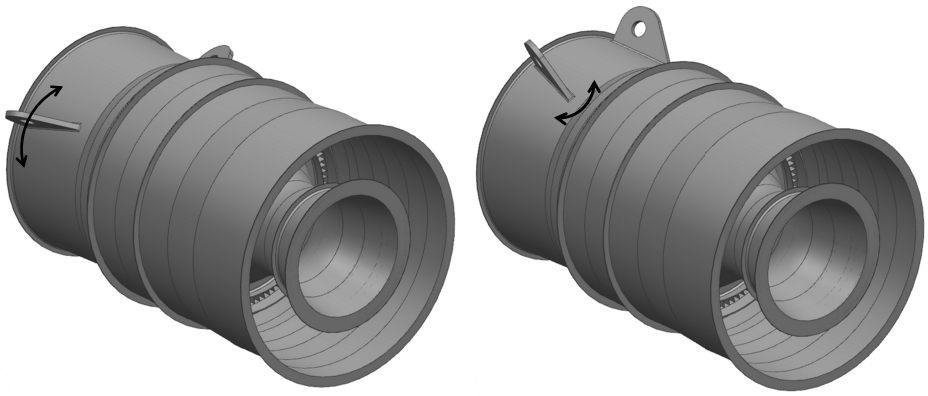

(a) (b)

Fig. 10 An illustration of the lower (a) and upper (b) limits and movement of the thrust linkage setting angle and circumferential position.

model. The general location and shape of the stress and rotordynamics constraint boundaries are also predicted well.

VIII. Two Variable Single & Multi-Fidelity Surrogate Models

As alluded to in the introduction and in the description of the Kriging and Co-Kriging models, it is the intention of this article to not only illustrate the feasibility of carrying out an optimization using WETTM simulations through the use of a surrogate modeling based approach but to illustrate the advantages that a multi-fidelity surrogate modeling approach can offer such an optimization.

To illustrate the accuracy with which both single and multi-fidelity surrogate modeling techniques predict the variation of SFC throughout the design space, consider the two variable design problem where the thrust linkage setting angle and circumferential position are altered by $\pm 15^{\circ}$ as indicated in Figure 10. In this case no rotor sub-optimization is to be performed and the SFC will therefore be calculated using a fixed set of transient displacements from the baseline rotor.

Figure 11(a) illustrates the "true" variation in SFC as the thrust linkage setting angle and circumferential position is altered. The surface plot, in this case, is a Kriging model constructed

Table 3 Comparison of 2D surrogate model accuracies.

Strategy	r^2			RMSE			MAE		
10pt Kriging	0.970	0.954	0.935	0.138	0.153	0.134	0.329	0.306	0.232
5pt Kriging	0.815	0.756	0.029	0.253	0.243	0.599	0.543	0.591	1.521
4pt + 30 Co-Kriging	0.979	0.925	0.846	0.093	0.169	0.555	0.159	0.418	1.407

from a total of 30 WETTM simulations. Unlike the 2D rotor optimization, the WETTM simulations are extremely expensive, it is therefore infeasible to perform a full factorial sampling to check the accuracy of any Kriging or Co-Kriging models produced. Instead the accuracy of these models will be assessed using the 30 sample points of Figure 11(a).

To compare the accuracy of single and multi-fidelity surrogate models in the prediction of this design space, a total of three different surrogate modeling strategies were assessed. Two strategies employed a single fidelity Kriging model with either five or ten Latin Hypercube sampling points. The multi-fidelity strategy involved the construction of a Co-Kriging model using a total of four WETTM simulations and 30 steady-state mechanical simulations. In these examples, the four point DoE is an optimal subset of the five point sampling plan which itself is an optimal subset of the ten point sampling plan as per the approach of Forrester et al.[28]. The Co-Kriging model is therefore identical in cost to the five point Kriging model with one sample point replaced by 30 cheap simulations of total equivalent cost. Latin Hypercube sampling plans, of course, have a random element to their definition which can impact on the results of such comparisons. To reduce this impact, three different surrogate models were constructed for each strategy.

Table 3 presents the r^2 correlations, RMSEs and MAEs for each of the three surrogate models for each strategy. Figure 11 illustrates the surrogate models resulting from the first surrogate iteration. The Co-Kriging model illustrated in Figure 11(d) is therefore based on a subset of four points from Figure 11(c) plus 30 low fidelity simulations and Figure 11(c) is constructed from a five points subset of the ten points used to construct the surrogate in Figure 11(b).

The results of Table 3 indicate that the additional information included within the multi-fidelity Co-Kriging model from the steady-state mechanical simulations creates a surrogate model which

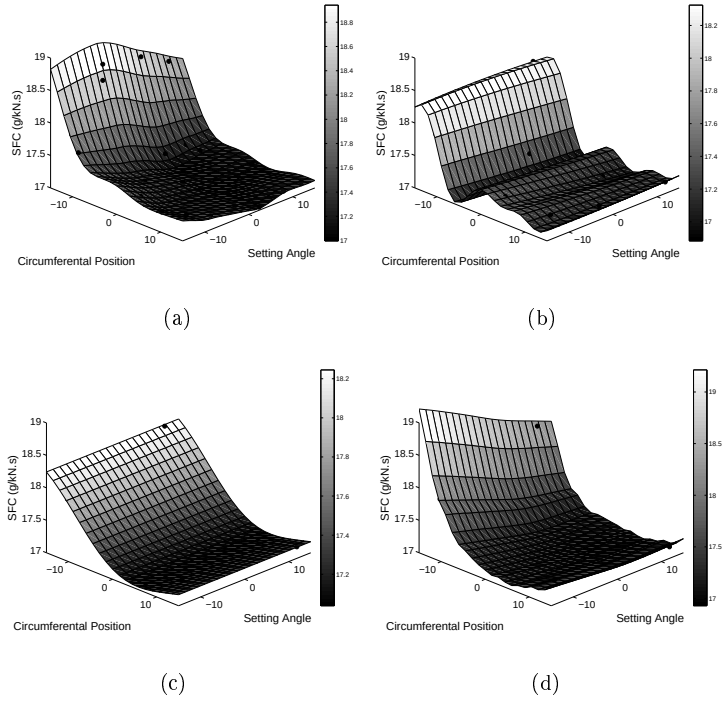

Fig. 11 Variation in SFC with changes in thrust linkage setting angle and circumferential position, "True"(a), 10pt Kriging(b), 5pt Kriging(c) & 4+30pt Co-Kriging models (d).

much more accurately represents the design space than an equivalent cost single fidelity model. The Co-Kriging model represents the variation in SFC so well that it even begins to approach the accuracy of a Kriging model constructed from ten sample points. The Co-Kriging model is therefore almost as accurate as a Kriging model which, in terms of WETTM simulations, is twice as expensive to construct.

Figure 11 reflects these results graphically. Of the three surrogate models illustrated, the multi-fidelity approach clearly results in a better prediction of the design space. It has the same general trend as the "true" response without the under prediction observed with the ten point Kriging model. The Co-Kriging and 10 point Kriging model appear to be similar in the statistics of Table 3 because there is no test sample point in the under prediction region of Figure 11(b). If there was, one might expect the accuracy of this model indicated in Table 3 to reduce.

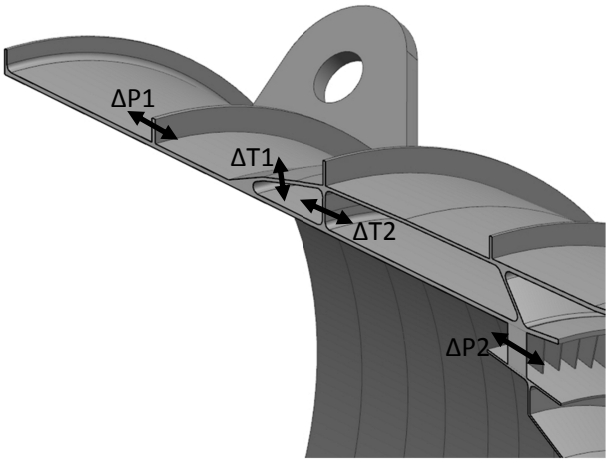

Fig. 12 Four variable engine parameterization.

IX. Four Variable Optimization

The previous section clearly demonstrated the advantages of multi-fidelity surrogate modeling in terms of its accuracy. Given the accuracy with which the Co-Kriging model represents the variation in SFC throughout the design space, it would be expected that an optimization employing such a surrogate would converge towards the optimum faster than an optimization employing a single fidelity model.

To investigate this, consider a four variable optimization of the engine casing. In this case, the axial position of an additional stiffening ring on the HPC casing, (ΔP1), the thickness of two casing sections, (ΔT1 & ΔT2), and the axial position of the aerodynamic struts at the exit of the compressor, (ΔP2), as illustrated in Figure 12, are all allowed to vary.

The optimization aims to minimize the SFC of the engine while constraining the total mass of the casing and rotor to be no greater than that of the baseline engine design. In this case, for every casing design considered, the rotor is redesigned in a sub-optimization which takes into account constraints on the rotor mass, stress, and rotordynamics performance. The rotor is therefore not permitted to be any heavier than the baseline rotor design and any saving in rotor mass can therefore be used to improve the casing design. Although not considered here, it would be possible to expand this optimization to include other constraints, or indeed, objective functions. Stresses in the casing,

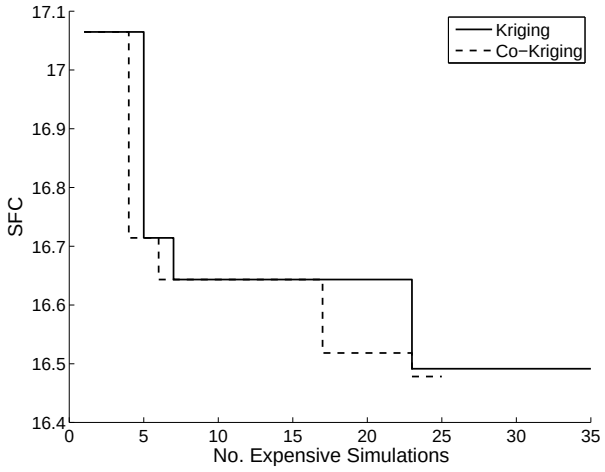

Fig. 13 Search history for a four variable engine optimization.

blade containment and other critical loading conditions could all be considered.

Two different optimization methodologies are used to improve the engine design. The first is a basic single fidelity surrogate modeling approach where an initial 20 point Latin Hypercube sampling plan is augmented by a number of update iterations based on surrogate models of SFC and total engine mass. The second approach is a multi-fidelity optimization where a 15 point Latin Hypercube sampling plan of WETTM simulations is augmented by 150 low fidelity steady-state mechanical simulations. To ensure a fair comparison between the two optimizations, the 15 point sample plan of the multi-fidelity optimization is an optimal subset of the 20 point sample plan used in the single fidelity optimization.

In both optimizations, five additional engine designs are analyzed per update iteration with one evaluated at the predicted optimum, two at points which maximize the expected improvement and two at points which maximize the predicted error in the surrogates. This mixture of approaches therefore ranges from full exploitation to a balanced exploitation/exploration using expected improvement and full exploration using the error prediction. In all cases, a binary encoded genetic algorithm with a population size of 50 is run for 50 generations to locate updates with a K-means clustering algorithm used to ensure that the updates are not adjacent to one another in the design

space. As per the 2D rotor optimization, these optimizations are carried out using the proprietary Rolls-Royce optimization software, OPTIMATv2.

The WETTM simulations carried out in both optimizations are performed on the University of Southampton Spitfire cluster where up to 47 WETTM or steady-state mechanical simulations can be performed in parallel. In the case of the single fidelity optimization, the entire 20 point DoE and each batch of five updates is evaluated in parallel. In the multi-fidelity optimization, the WETTM simulations from the 15 point DoE are all evaluated in parallel while the 150 low fidelity simulations are performed in batches of 30. This means that all of the low fidelity simulations can be performed in approximately 17 hours, well before any of the WETTM DoE simulations have completed. Each of the five update points for the multi-fidelity optimization are evaluated using both WETTM simulations and steady-state mechanical simulations to maintain the accuracy of the Co-Kriging difference model.

Figure 13 presents the search history for both the Kriging and Co-Kriging optimizations. As the optimization aims to improve SFC as predicted by WETTM simulations, only the results of these simulations are presented in Figure 13.

Both optimizations offer an improvement over the SFC of the baseline engine of 17.065 with the Kriging based optimization improving SFC by 3.36% and the Co-Kriging based optimization improving SFC slightly more, by 3.44%. Looking at the optimization histories, it appears that immediately after the completion of their respective DoEs both optimizations find very good designs within their initial set of five updates. However, once the Kriging model has found this design, it is unable to improve upon it further. After evaluating two more batches of updates, which equates to 8.7 days of additional compute time compared to the Co-Kriging model, the Kriging model has still not improved over the initial design.

Both optimizations result in somewhat similar designs. The positions of the additional stiffening ring and aerodynamic strut are almost identical with a difference of less than 1.0mm in their positioning. The casing thicknesses, however, are more substantially different with the Co-Kriging optimization having a larger ΔT1 at the expense of a smaller ΔT2 compared to the final Kriging design. The mass of the Co-Kriging design is also closer to the 1605.72kg mass constraint than the

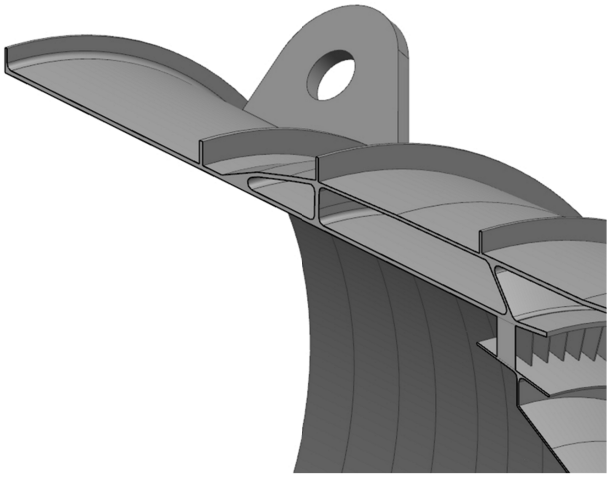

Fig. 14 Final improved engine design.

Kriging design. The Co-Kriging optimization achieves a final mass of 1605.68kg while the Kriging design achieves a mass of 1605.56kg. The final design from the Co-Kriging optimization is illustrated in Figure 14.

In both cases the optimization is attempting to maintain a total mass no greater than the mass of the baseline design which did not have an additional stiffening ring present. The rotor sub-optimization has therefore, in both cases, resulted in a reduction in rotor mass which has then been spent, in conjunction with adjustments to the casing thicknesses, maintaining the mass constraint while improving SFC.

X. Conclusion

A multi-disciplinary whole engine design optimization was performed resulting in a 3.44% improvement in the SFC of the test engine for no additional mass. This design was obtained through simultaneous consideration of the engine rotor and casing within a bi-level multi-fidelity optimization framework. This study has therefore successfully illustrated:

1. The feasibility of employing 3D transient whole engine thermo-mechanical simulations within a design optimization.

2. The advantages of employing a multi-fidelity approach within such a design optimization to improve the efficiency of the optimization and the quality of the final design.

3. The advantages of a programmatic approach to parameterization when maintaining the continuity of surface tags for the correct application of boundary conditions after topological changes, is a priority.

4. An efficient rotor sub-optimization employing surrogate models of rotor mass, Von Mises stress, rotordynamics performance and a POD based representation of rotor platform transient displacements.

5. The advantages of considering a holistic approach to gas turbine engine design optimization by allowing trade-offs between rotor and casing mass.

While the complexity of the engine geometry, load cases and the number of objectives and constraints considered here could be considered some way short of a real life gas turbine design process, the present study never-the-less demonstrates the potential for such holistic, multi-fidelity, multi-disciplinary, design optimizations to positively impact the performance of the next generation of gas turbines.

Moving forward, there are a number of areas in which the present study could be expanded upon, or improved. The current study considers only the HPC tip clearances and their impact on SFC, but given the fact that a whole engine simulation is employed the impact of other compressor or turbine stages and even bearings and seals on SFC could be included within the optimization. Additional loading conditions, constraints and other analysis disciplines could also be included within the workflow. Likewise only a minor adjustment of the formulation of the presented optimization problem is required to solve a mechanical or weight problem for a fixed SFC. The entire workflow could even be recast as a multi-objective optimization problem thereby providing the designer with a set of Pareto optimal designs which trade-off efficiency, weight and structural performance. The current approach has also been designed around a number of limitations in the current design and analysis tools which could be improved upon. For example, the presented multi-fidelity approach employed an identical mesh in both the WETTM and mechanical analysis, the mesh could be more

efficiently generated to reduce the degrees of freedom and different meshes could also be used by the different simulation fidelities to further reduce cost. The scheme of Makem et al.[6], for example, could be employed in this workflow to reduce the cost of the optimization to considerable effect. Similarly, alternative low fidelity schemes could be considered such as the dimensional reduction process of Nolan et al.[42]. The idea of computing the faces to which analysis attributes are to be applied[16] could also be used to ensure the model updating is robust against topology changes.

The application of surrogate modelling approaches within such optimizations relies on the accuracy and applicability of the physical model upon which the surrogates are built and, in the case of a multi-fidelity surrogate, on the correlation between the different model fidelities. Employing such large and complex simulations within a design optimization naturally introduces issues regarding the accuracy of the underlying simulations in the extremum of the design space. The efficient capturing of uncertainties in both the geometry and the modelling of the physics is therefore an important area for further research which may prevent the optimizer from exploiting flaws in the underlying simulation.

Acknowledgments

The research leading to these results has received funding from the European Community's Seventh Framework Programme (FP7/2007-2013) under grant agreement no. 234344 (www.crescendo-fp7.eu).

References

[1] Eisenlohr, G. and Chladek, H., "Thermal Tip Clearance Control for Centrifugal Compressor of an APU Engine," *Journal of Turbomachinery*, Vol. 116, No. 4, 1994, pp. 629–634, doi:10.1115/1.2929453.

[2] Benito, D., Dixon, J., and Metherell, P., "3D Thermo-Mechanical Modelling Method to Predict Compressor Local Tip Running Clearances," in "Proceedings of the ASME Turbo Expo 2008: Power for Land, Sea, and Air, Berlin, Germany, June 9-13th," , 2008.

[3] Arkhipov, A., Karaban, V., Putchkov, I., Filkorn, G., and Kieninger, A., "The Whole-Engine Model for Clearance Evaluation," in "Proceedings of ASME Turbo Expo 2009: Power for Land, Sea and Air, Orlando, Florida, USA, June 8-12," , 2009.

[4] Lee, C., Song, J., Lee, S., and Hong, D., "Effect of a Gap Between Inner Casing and Stator Blade on Axial Compressor Performance," in "Proceedings of ASME Turbo Expo 2010: Power for Land, Sea and Air, Glasgow, UK, June 14-18," , 2010.

[5] Voutchkov, I., Keane, A., and Fox, R., "Robust Structural Design of a Simplified Jet Engine Model Using Multiobjective Optimization," in "11th AIAA/ISSMO Multidisciplinary Analysis and Optimization Conference, Portsmouth, Virginia, USA, September 6-8," , 2006.

[6] Makem, J., Armstrong, C., and Robinson, T., "Automatic decomposition and efficient semi-structured meshing of complex solids," *Engineering with Computers, 2012*, pp. 1–17, doi:10.1007/s00366-012-0302-x.

[7] Goldberg, D., *Genetic Algorithms in Search, Optimization & Machine Learning*, Addison-Wesley, 1989.

[8] Kirkpatrick, S., Gelatt, C., and Vecchi, M., "Optimization by Simulated Annealing," *Science*, Vol. 220, 1983, pp. 671–680, doi:10.1126/science.220.4598.671.

[9] Brooks, C., Forrester, A., Keane, A., and Shahpar, S., "Multi-Fidelity Design Optimisation of a Transonic Compressor Rotor," in "9th European Turbomachinery Conference, Istanbul, Turkey, 21st-25th March," , 2011.

[10] Kuya, Y., Takeda, K., Zhang, X., and Forrester, A., "Multifidelity Surrogate Modeling of Experimental and Computational Aerodynamic Data Sets," *AIAA Journal*, Vol. 49, No. 2, 2011, pp. 289–298, doi:10.2514/1.53410.

[11] Toal, D. and Keane, A., "Efficient Multi-Point Aerodynamic Design Optimization Via Co-Kriging," *Journal of Aircraft*, Vol. 48, No. 5, 2011, pp. 1685–1695, doi:10.2514/1.C031342.

[12] Wankhede, M., Bressloff, N., and Keane, A., "Combustor Design Optimization Using Co-Kriging of Steady and Unsteady Turbulent Combustion," *Journal of Engineering for Gas Turbines and Power*, Vol. 133, No. 12, doi:10.1115/1.4004155.

[13] Han, Z., Zimmermann, R., and Görtz, S., "Alternative CoKriging Model for Variable-Fidelity Surrogate Modeling," *AIAA Journal*, Vol. 50, No. 5, 2012, pp. 1205–1210, doi:10.2514/1.1051243.

[14] Bettebghor, D., Blondeau, C., Toal, D. J., and Eres, H., "Bi-Objective Optimization of Pylon-Engine-Nacelle Assembly: Weight vs. Tip Clearnce Criterion," *Structural and Multidisciplinary Optimization*, Vol. 48, No. 3, 2013, pp. 637–652,

doi:10.1007/s00158-013-0908-7.

[15] Cao, Y., Zhou, A., Wu, H., and Cheng, H., "Development of feature recognition and extraction system based on NX platform," in "Proceedings of the 2nd International Conference on Electronic and Mechanical Engineering and Information Technology, EMEIT 2012," , 2012.

[16] Nolan, D., Tierney, C., Robinson, T., and Armstrong, C., "Defining Simulation Intent," in "NAFEMS European Conference: Simulation Process and Data Management (SDM), Munich, Germany," , 2011.

[17] Sacks, J., Welch, W., Mitchell, T., and Wynn, H., "Design and Analysis of Computer Experiments," *Statistical Science*, Vol. 4, No. 4, 1989, pp. 409–435,
doi:10.2307/2245858.

[18] Simpson, T., Peplinski, J., Kock, P., and Allen, J., "Metamodels for Computer-based Engineering Design: Survey and Recommendations," *Engineering with Computers*, Vol. 17, No. 2, 2001, pp. 129–150,
doi:10.1007/PL00007198.

[19] Queipo, N., Haftka, R., Shyy, W., Goel, T., Vaidyanathan, R., and Tucker, P., "Surrogate-based analysis and optimization," *Progress in Aerospace Sciences*, Vol. 41, 2005, pp. 1–28,
doi:10.1016/j.paerosci.2005.02.001.

[20] Forrester, A. and Keane, A., "Recent advances in surrogate-based optimization," *Progress in Aerospace Sciences*, Vol. 45, No. 1-3, 2009, pp. 50–79,
doi:10.1016/j.paerosci.2008.11.001.

[21] Jones, D., "A Taxonomy of Global Optimization Methods Based on Response Surfaces," *Journal of Global Optimization*, Vol. 21, No. 4, 2001, pp. 345–383,
doi:10.1023/A:1012771025575.

[22] Toal, D., Bressloff, N., Keane, A., and Holden, C., "The Development of a Hybridized Particle Swarm for Kriging Hyperparameter Tuning," *Engineering Optimization (Accepted for Publication)*,
doi:10.1080/0305215X.2010.508524.

[23] Keane, A., "Statistical Improvement Criteria for Use in Mulitobjective Design Optimization," *AIAA Journal*, Vol. 44, No. 4, 2006, pp. 879–891.

[24] Toal, D., Forrester, A., Bressloff, N., Keane, A., and Holden, C., "An Adjoint For Likelihood Maximization," *Proceedings of the Royal Society A*, Vol. 465, No. 2111, 2009, pp. 3267–3287,
doi:10.1098/rspa.2009.0096.

[25] Toal, D. and Keane, A., "Non-Stationary Kriging for Design Optimization," *Engineering Optimization*,
doi:10.1080/0305215X.2011.607816.

[26] Jones, D., Schonlau, M., and Welch, W., "Efficient Global Optimization of Expensive Black-Box Functions," *Journal of Global Optimization*, Vol. 13, No. 4, 1998, pp. 455–492, doi:10.1023/A:1008306431147.

[27] Kennedy, M. and O'Hagan, A., "Predicting the Output from a Complex Computer Code When Fast Approximations are Available," *Biometrika*, Vol. 87, No. 1, 2000, pp. 1–13, doi:10.1093/biomet/87.1.1.

[28] Forrester, A., Sóbester, A., and Keane, A., "Multi-Fidelity Optimization via Surrogate Modelling," *Proceedings of the Royal Society A*, Vol. 463, No. 2088, 2007, pp. 3251–3269, doi:10.1098/rspa.2007.1900.

[29] Armstrong, I. and Edmunds, T., "Fully Automatic Analysis in the Industrial Environment," in "Proceedings of Second International Conference on Quality Assurance in Finite Element Analysis, NAFEMS, Stratford-upon-Avon, England, May 22-25," , 1989.

[30] Alexiou, A. and Mathioudakis, K., "Development of Gas Turbine Performance Models Using a Generic Simulation Tool," in "ASME Turbo Expo 2005: Power for Land, Sea, and Air, Reno, Nevada, USA, June 6-9," , 2005, doi:10.1115/GT2005-68678.

[31] Alexiou, A. and Mathioudakis, K., "Gas Turbine Engine Performance Model Applications Using An Object-Oriented Simulation Tool," in "ASME Turbo Expo 2006: Power for Land, Sea, and Air, Barcelona, Spain, May 8-11," , 2006, doi:10.1115/GT2006-90339.

[32] Choi, B. and Yang, B., "Optimum Shape Design of Rotor Shafts Using Genetic Algorithm," *Journal of Vibration and Control*, Vol. 6, No. 2, 2000, pp. 207–222, doi:10.1177/107754630000600203.

[33] Choi, B. and Yang, B., "Multiobjective Optimum Design of Rotor-Bearing Systems With Dynamic Constraints Using Immune-Genetic Algorithm," *Journal of Engineering for Gas Turbines and Power*, Vol. 123, No. 1, 2001, pp. 78–81, doi:10.1115/1.1338952.

[34] Kim, Y.-H., Tan, A., Yang, B.-S., Kim, W.-C., Choi, B.-K., and An, Y.-S., "Optimum Shape Design of Rotating Shaft by ESO Method," *Journal of Mechanical Science and Technology*, Vol. 21, No. 7, 2007, pp. 1039–1047, doi:10.1007/BF03027653.

[35] Strauß, F., Inagaki, M., and Starke, J., "Reduction of Vibration Level in RRotordynamic by Design

Optimization," *Structural and Multidisciplinary Optimization*, Vol. 34, No. 2, 2007, pp. 139–149, doi:10.1007/s00158-006-0065-3.

[36] Ressing, H. and Kukla, S., "Improving Rotordynamic Performance of an Axial Flow Compressor with Two-Lobe Bearings Using Nonlinear Constraint Parameter Optimization," in "Proceesings of ASME 2011 Turbo Expo: Turbine Technical Conference and Exposition, Vancouver, British Columbia, Canada, June 6-10," , 2011.

[37] Ritto, T., Lopez, R., Sampaio, R., and Souza de Cursi, J., "Robust Optimization of a Flexible Rotor-Bearing System Using the Campbell Diagram," *Engin*, Vol. 43, No. 1, 2011, pp. 77–96, doi:10.1080/03052151003759125.

[38] Toal, D. and Keane, A., "Non-Stationary Kriging Prediction of the Performance of Turbomachinery Components," in "European Turbomachinery Conference, Istanbul, Turkey, March $21^{\text{st}} - 25^{\text{th}}$," , 2011.

[39] Xiao, M., Breitkopf, P., Coelho, R., Knopf-Lenoir, C., Sidorkiewicz, M., and Villon, P., "Model Reduction by CPOD and Kriging: Application to the shape optimization of an intake port," *Structural and Multidisciplinary Optimization*, Vol. 41, No. 4, 2010, pp. 555–574, doi:10.1007/s00158-009-0434-9.

[40] Sirovich, L., "Turbulence and Dynamics of Coherent Structures Part 1: Coherent Structures," *Quarterly of Applied Mathematics*, Vol. 45, No. 3, 1987, pp. 561–571.

[41] Morris, M. and Mitchell, T., "Exploratory Designs for Computational Experiments," *Journal of Statistical Planning and Inference*, Vol. 43, No. 3, 1995, pp. 381–402.

[42] Nolan, D., Tierney, C., Armstrong, C., Robinson, T., and Makem, J., "Automatic dimensional reduction and meshing of stiffened thin-wall structures," *Engineering with Computers, 2013*, doi:10.1007/s00366-013-0317-y.

[43] http://www.plm.automation.siemens.com

[44] http://www.lmsintl.com/rotor-dynamics